Fermi-edge singularity and related emission from degenerate semiconductors: Transition from a spontaneous to a stimulated process

Aika Tashiro,[1] Toshihiro Nakamura,[2] Yutaka Adachi,[3] Yoshiki Wada,[3] and Takashi Uchino[1]
[1]*Department of Chemistry, Kobe University, Nada, Kobe 657-8501, Japan*
[2]*Department of Electronic and Electronics, Hosei University, Koganei, Tokyo 184-8584, Japan*
[3]*Optical and Electronic Materials Unit, National Institute for Materials Science, Namiki 1-1, Tsukuba 305-0044, Japan*

(Received 6 September 2023; revised 17 November 2023; accepted 4 January 2024; published 2 February 2024)

We report on the observation of Fermi-edge singularity in the optical absorption and emission spectra of high-quality degenerate Ga-doped ZnO (GZO) films from cryogenic to room temperature, as well as on the related stimulated emission under femtosecond laser pulse excitation. When the photogenerated electron-hole pair density n_p reaches a threshold, which is as low as $n_p \approx 10^{19}$ cm^{-3} at room temperature, the emission from the Fermi edge shows a transition from a spontaneous to a stimulated regime, accompanied by a blueshift in the emission maximum. Further increase in the excitation fluence not only leads to a substantial increase in emission intensity, but it also results in broad and redshifted spectra, accompanied by the shortening of decay times. The resulting stimulated emission can be interpreted in terms of the emission of a population-inverted electron-hole plasma (EHP) in the weakly excited degenerated GZO. The observed low-threshold EHP stimulated emission is consistent with the calculated gain spectra based on a quantum many-body theory.

DOI: 10.1103/PhysRevB.109.075302

I. INTRODUCTION

In solid state physics, many-body effects, which are ultimately related to the correlation among electrons, are one of the most interesting, but also the most challenging, issues both in terms of experiments and theoretical treatments [1–4]. The primary difficulty is that a large number of electrons can interact through the infinite-range Coulomb force on an extremely short timescale ($\approx 10^{-12}$ s), enabling a coherent superposition of eigenstates not found in "free-electron" systems [3]. In photoexcited semiconductors, things will become more complicated because of the generation of photoexcited electrons and holes simultaneously. This leads to the formation of excitons or an electron-hole plasma (EHP) state depending on the density of the electron-hole pair [5]. In the Mott transition model, the exciton bound states cease to exist when the electron-hole pair density n_p exceeds the Mott density n_M [5]. In view of many-body physics, however, an excitonlike effect still survives even for $n_p < n_M$ due to the many-electron/one-hole interaction in the presence of the Fermi sea, which yields a "many-body" exciton, or a Mahan exciton [6]. Also, a divergence of optical oscillator strength occurs at the Fermi level of highly doped and highly excited semiconductors, giving rise to a so-called Fermi-edge singularity (FES) in optical absorption and emission spectra [7]. Thus, the observation of the FES and the Mahan exciton has been regarded as a hallmark of many-body effects and is still a topic of active research in the field of condensed matter physics [8–20].

Although the FES has been reported to occur in various degenerate semiconductors, including highly doped bulk [8–10,21–30] and modulation-doped quantum wells [31–35], stimulated light emission from the Fermi edge has hardly been observed. This appears to be strange because in degenerate semiconductors, their chemical potential is located well within the conduction (or valence) band already in equilibrium. According to the Bernard and Duraffourg (B-D) condition [36], the EHP gain at a temperature T is achieved when the electron-hole pair chemical potential μ with respect to the band gap ($\mu = \mu_e + \mu_h$) becomes greater than $\approx 2k_BT$ [36,37], where μ_e (μ_h) is the quasichemical potential for electrons (holes) measured from the conduction(valence)-band edge and k_B is the Boltzmann constant. The B-D condition implies that the optical gain from an inverted EHP state could be in principle achieved for much lower values of n_p than that of the intrinsic one [38]. A possible reason for the difficulty in observing the Fermi-edge stimulated emission is that high doping induces lattice defects/strains and related nonradiative centers, which would potentially prevent the optical amplification. In the case of the modulation-doped quantum wells, the FES and the related emission tend to be removed when the density of photoexcited carriers is increased to a certain level due to the significant state broadening and damping of photoexcited holes [32]. Hence, the Fermi-edge stimulated emission is challenging to be realized, but it is worth investigating as it will provide insight into many-body effects and the related optical emission features in degenerate semiconductors.

In this paper, we overcome the problem using high-quality degenerate Ga-doped ZnO (GZO) films prepared by a pulsed laser deposition (PLD) method in highly optimized and controlled conditions. Previously, lasing characteristics of ZnO thin films, nanowires, and nanoparticles were intensively investigated [39–45]. The threshold value of n_p for EHP lasing for nominally undoped ZnO nanosystems is reported to be as high as $\approx 10^{19} - 10^{20}$ cm^{-3} at room temperature [44,45], while the value of n_M is estimated to be $\approx 2-6 \times 10^{18}$ cm^{-3} at 300 K [46–48]. Although the FES was reported from highly

doped ZnO films with a carrier concentration higher than n_M [10], stimulated emission from the Fermi edge has not yet been reported. Here, we performed detailed optical absorption and photoluminescence (PL) measurements on the high-quality degenerate GZO samples from cryogenic to room temperature, along with calculations based on a quantum many-body theory. We then found that the present samples not only show the signature of the FES in the absorption and emission spectra, but they also demonstrate a transition from a spontaneous to a stimulated regime under relatively low excitation conditions even at room temperature.

II. EXPERIMENTAL AND CALCULATIONAL PROCEDURES

A. Sample preparation

In this paper, ZnO and Ga-doped ZnO thin films were fabricated on an *a*-plane sapphire substrate by the PLD technique. The targets were polycrystalline pellets of pure ZnO and Ga-doped ZnO prepared by sintering of ZnO-Ga_2O_3 mixture powders. The nominal Ga concentrations of the targets were varied from 0.05 to 2 at. % to obtain GZO films with different carrier concentrations. The principal advantages of PLD are its ability to create high-energy source particles as well as its simple experimental setup, enabling high-quality film growth at low substrate temperatures (typically 200–800 °C). Although PLD is conceptually simple, there are a number of parameters to be optimized, e.g., laser fluence, substrate temperature, background process atmosphere, and the type of substrate, for the synthesis of high-quality films [49]. As for the growth parameters of pure ZnO thin films, optimum conditions have been developed to obtain epitaxial thin films with high crystalline quality. However, the fabrication of high-quality Ga-doped ZnO (GZO) thin films, especially degenerate GZO ones, is much more challenging than that of pure ZnO thin films. After many trials and errors, we were able to create high-quality degenerate GZO films with a carrier density up to $\approx 2 \times 10^{20} \mathrm{cm}^{-3}$ using a KrF excimer laser (Coherent, COMPex50; wavelength $\lambda = 248$ nm, repetition rate = 5 Hz, pulse width = ≈20 ns) for the laser ablation process. The optimal substrate temperature and oxygen pressure are 450 °C and 1.1×10^{-5} Torr, respectively. We found that the type of laser is especially important to obtain high-quality GZO films. When we used the fourth harmonic ($\lambda =$ 266 nm) of a Nd-doped yttrium aluminum garnet (Nd:YAG) laser with a pulse width of 5 ns, we did not obtain high-quality GZO thin films but observed an impurity-related absorption at the absorption edge. The PLD growth on *a*-plane sapphire is also essential to suppress the formation of in-plane rotation domains or twins [50,51], which are often introduced in ZnO thin films grown on a *c*-plane sapphire substrate.

B. Characterization

The crystallinity of the film samples was characterized by x-ray diffraction with a PANalytical X'pert Pro Materials Research Diffractometer equipped with a hybrid two-bounce asymmetric Ge (220) monochromator and CuK_α source. The optical absorption of the films was measured using a monochromated Xe lamp and a lock-in amplifier with optical chopper. The temperature of the sample loaded in a He-flow cryostat was controlled with a temperature controller (Lakeshore 330) in the temperature range from 6 to 300 K. Steady state PL and PL excitation (PLE) spectra were measured with a spectrofluorometer (JASCO, FP6600) equipped using a cold finger cryostat and a Xe lamp as an excitation source. For the Hall measurements, the standard van der Pauw geometry was used with an excitation current of 1 mA. The offset of voltage was eliminated by reversing the direction of magnetic field during the measurement. Time integrated PL (TIPL) and time-resolved PL (TRPL) measurements on the GZO samples were carried out with a femtosecond Ti:sapphire laser system with an optical parametric amplifier (OPA). We used the 332-nm pulses generated with the OPA (Spectra Physics, TOPAS prime), which was seeded by a 1-kHz Ti:sapphire regenerative amplifier system (Spectra Physics, Mai Tai SP and Solstice) producing 100-fs pulses at 800 nm. This femtosecond-laser system, combined with a streak camera (Hamamatsu Photonics, C5680), was used to obtain TIPL and TRPL spectra. The overall time resolution of the measuring system was ≈100 ps. For the TIPL and TRPL measurements, the samples were excited by a 100-fs laser pulse focused to a spot area of 0.325 mm^2, and the emission signal from the front surface was monitored. The sample temperature was controlled in a He-flow cryostat system in the temperature range from 6 to 300 K. The excitation fluence can be varied up to 2.2 $\mathrm{mJ/cm}^2$, which is sufficient to observe stimulated emissions from the GZO samples. However, this femtosecond-laser system is not suitable to investigate the stimulated emission properties of the pure ZnO thin film as its threshold fluence is a few $\mathrm{mJ/cm}^2$ at room temperature. Hence, for the pure ZnO thin film, we used the third harmonic ($\lambda = 355$ nm) of a high-power 10-ns *Q*-switched Nd-doped yttrium aluminum garnet (Nd:YAG) laser (Spectra Physics, INDI-40, repetition rage 10 Hz) as an excitation source. Using this nanosecond-laser system, the excitation fluence can be increased up to ≈50 $\mathrm{mJ/cm}^2$, which is high enough to observe the room-temperature stimulated emission from the pure ZnO thin film.

C. Numerical calculations of quasichemical potentials for electrons and holes

In this paper, μ_e and μ_h in the photoexcited *n*-type semiconductors for electron density n ($n = n_p + n_d$) and hole density p ($p = n_p$) were numerically determined from the following equations within the parabolic band approximation:

$$n = n_p + n_d = \frac{1}{2\pi^2}\left(\frac{2m_e}{\hbar^2}\right)^{\frac{3}{2}} \int_0^\infty \frac{\sqrt{\varepsilon}}{\exp\left(\frac{\varepsilon-\mu_e}{k_B T}\right)+1} d\varepsilon, \quad (1)$$

$$p = n_p = \frac{1}{2\pi^2}\left(\frac{2m_e}{\hbar^2}\right)^{\frac{3}{2}} \int_0^\infty \frac{\sqrt{\varepsilon}}{\exp\left(\frac{\varepsilon-\mu_h}{k_B T}\right)+1} d\varepsilon, \quad (2)$$

where m_e and m_h are the electron and hole effective masses, respectively, and $\hbar$ is the reduced Planck constant ($\hbar = h/2\pi$). Although the change in the shape of the conduction band is likely to occur in degenerately *n*-doped semiconductors [22], we did not take into account the possible nonparabolic nature of the conduction band but employed the energy-independent

effective masses, i.e., $m_e = 0.28m_0$ and $m_h = 0.59m_0$ [46], where m_0 is the free electron mass.

D. Gain calculation

In the present paper, we calculated the optical gain spectra $g(E)$ based on a many-body theory developed by Versteegh *et al.* [46]. In brief, the $g(E)$ at a photon energy E is directly obtained from the imaginary part of the complex susceptibility $\chi(E)$ as follows:

$$g(E) = -\frac{2E}{\hbar c}\mathrm{Im}[\sqrt{1+\chi(E)}], \tag{3}$$

where c is the speed of light in vacuum. The susceptibility $\chi(E)$ is given by

$$\chi(E) = \chi_L + \frac{2d_{cv}s}{(2\pi)^3\varepsilon_0}\sum_{k=0,s,\ldots}^{k_{\max}} 4\pi k^2\chi_k(E), \tag{4}$$

ε_0, χ_L, and d_{cv} represent the permittivity of vacuum, background susceptibility, and the dipole moment for the valence–conduction band transition, respectively. In this paper, we used $\chi_L = 2.4$ and $d_{cv} = 4.4 \times 10^{-29}$ cm. The s and $k_{\max}$ are the step size and the upper limit, respectively. The term $\chi_k(E)$ reads as

$$\chi_k(E) = -\Gamma_k(E)d_{cv}\frac{1-\left\{1+\exp\left[\frac{\epsilon_{k,e}-\mu_e}{k_BT}\right]\right\}^{-1}-\left\{1+\exp\left[\frac{\epsilon_{k,h}-\mu_h}{k_BT}\right]\right\}^{-1}}{E+i\hbar\gamma(E)-\epsilon_{k,e}-\epsilon_{k,h}-E_g}, \tag{5}$$

where E_g, $\epsilon_{k,e(h)}$, and $\gamma(E)$ are the band-gap energy, the kinetic energy of the electrons (holes), and the energy dependent damping parameter, respectively. The energy dependent damping parameter $\Gamma_k(E)$ is the vertex function, representing the screened Coulomb interactions, and it is calculated from a matrix inversion method [45].

The band-gap energy E_g is known to be dependent on the carrier density due to the band-gap renormalization effect. For taking into account the effect, we used the equation [45,46]

$$E_g = E_{g0} - \frac{E_{b_0}a_0}{\lambda_s}, \tag{6}$$

where E_{g_0} (3.38 eV), E_{b_0} (60 meV), and a_0 (1.83 nm) are the intrinsic band gap energy, the exciton binding energy and Bohr radius, respectively, for pure ZnO [45,46]. The screening length λ_s is obtained from the carried density dependent chemical potentials, μ_e and μ_h [45].

The damping parameter $\gamma(E)$ is calculated from the empirical function,

$$\gamma(E) = \frac{\gamma_0}{\exp[(-E+E_g-E_\alpha)/E_\alpha]+1}, \tag{7}$$

where E_α and γ_0 denote constants, and their values are 22 and 50 meV, respectively [46]. We should note that, we neglect the possible effect of defect/strain induced absorption in calculating $g(E)$. Hence, the thus obtained $g(E)$ gives the theoretical upper bound for the chosen parameters.

III. RESULTS AND DISCUSSION

A. Structural and transport properties

All the ZnO and GZO thin films are c axis oriented [Fig. 1(a)]. For the GZO films with n_d from 8.7×10^{19} to $2.0 \times 10^{20}\mathrm{cm}^{-3}$, the full width at half maximum values of x-ray rocking curves for the (0002) diffraction are comparable to that of the ZnO thin film [Fig. 1(b)]. Note also that the carrier Hall mobility η is as high as $50-80\,\mathrm{cm}^2\,\mathrm{V}^{-1}\,\mathrm{s}^{-1}$ for the GZO films with n_d around $1.0 \times 10^{20}\mathrm{cm}^{-3}$, whereas η decreases down to approximately $20\,\mathrm{cm}^2\,\mathrm{V}^{-1}\,\mathrm{s}^{-1}$ with a further increase in n_d up to $\approx 1 \times 10^{21}\mathrm{cm}^{-3}$ (Fig. 2). These results demonstrate that the high crystallinity is retained in our GZO samples as long as n_d is below $2 \times 10^{20}\mathrm{cm}^{-3}$, which is two orders higher than n_M in ZnO ($n_M \approx 2-6 \times 10^{18}\,\mathrm{cm}^{-3}$ at 300 K [46–48]).

B. Optical absorption and emission spectra

Figure 3(a) shows room-temperature optical absorption spectra for the ZnO film with the thickness $D = 249$ nm and $n_d = 2.7 \times 10^{16}\mathrm{cm}^{-3}$ and three GZO films, which are termed GZO1 ($D = 236$ nm, $n_d = 8.7 \times 10^{19}\mathrm{cm}^{-3}$), GZO2 ($D = 140$ nm, $n_d = 1.3 \times 10^{20}\mathrm{cm}^{-3}$), and GZO3 ($D = 320$ nm, $n_d = 8.3 \times 10^{20}\mathrm{cm}^{-3}$). The ZnO film shows typical sharp exciton-related absorption peaks in the $3.3-3.4$-eV energy range [39–43]. On the other hand, such excitonic features are missing in the GZO samples; rather, the absorption spectra of GZO1 and GZO2 are characterized by a steep rise at the absorption edge and a slow fall at higher energies, which is a typical characteristic of the FES. Makino *et al.* [10] demonstrated that the absorption spectrum $A(E)$ showing the FES in degenerate ZnO can be described by the following power-law function [7] convoluted with a Gaussian distribution with a

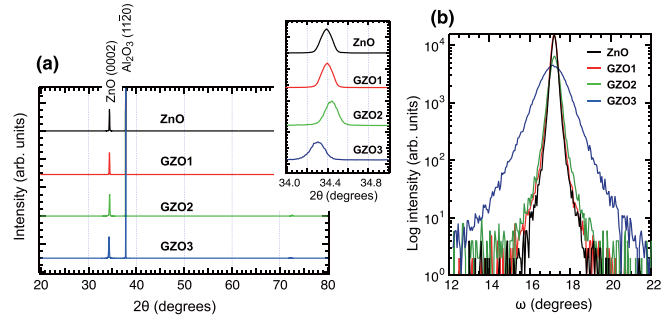

FIG. 1. (a) X-ray 2θ scans and (b) the (0 0 0 2) plane rocking curves of ZnO film ($D = 249$ nm and $n_d = 2.7 \times 10^{16}\mathrm{cm}^{-3}$) and three degenerate GZO films, termed GZO1 ($D = 236$ nm, $n_d = 8.7 \times 10^{19}\mathrm{cm}^{-3}$), GZO2 ($D = 140$ nm, $n_d = 1.3 \times 10^{20}\mathrm{cm}^{-3}$), and GZO3 ($D = 320$ nm, $n_d = 8.3 \times 10^{20}\mathrm{cm}^{-3}$). The inset in (a) is an expanded plot near the ZnO (0 0 0 2) diffraction peak.

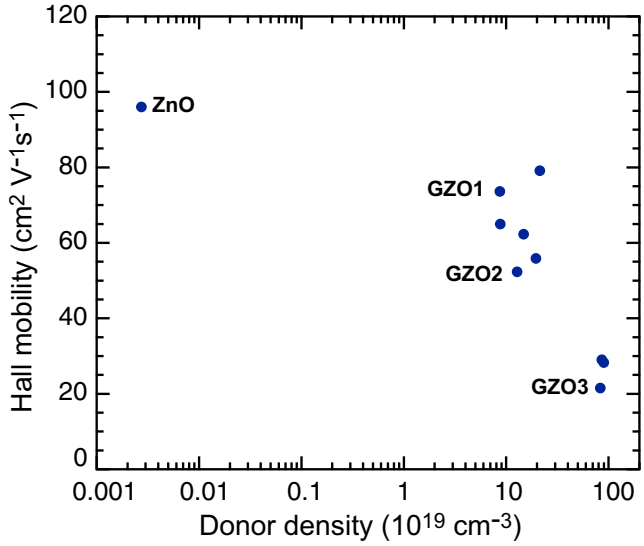

FIG. 2. Room-temperature Hall mobility of the PLD-grown thin films with different carrier densities. The values corresponding to the samples of ZnO, GZO1, GZO2, and GZO3 are indicated.

half width Γ_{Gauss} [9]:

$$A(E) = A_0(E) \int_{-\infty}^{+\infty} \left(\frac{\zeta_0}{E - E' - E_{\text{th}}} \right)^{\alpha} \times \exp\left\{ -\left(\frac{E'}{\Gamma_{\text{Gauss}}} \right)^2 \right\} dE', \tag{8}$$

where E is the energy of the photon, α is the coupling parameter related to the strength of the attractive electron-hole interaction, ζ_0 is a cutoff energy, and E_{th} is the threshold energy where the optical absorption sets in and hence reflects the Fermi edge [7]. The term $A_0(E)$ contains the factor derived from the fundamental absorption [10,52,53] as follows:

$$A_0(E) \propto \left[\frac{E_b \Gamma_0}{(E_0 - E_b - E)^2 + \Gamma_0^2} + \int_{E_0}^{+\infty} \frac{1}{1 - \exp[-2\pi z(E')]} \frac{\Gamma_0 dE'}{(E - E')^2 + \Gamma_0^2} \right], \tag{9}$$

where E_0 is the value of the fundamental band gap, Γ_0 is the broadening parameter, $z(E) = \{E_b/(E - E_0)\}^{1/2}$, and E_b is the exciton binding energy. The first and second terms in Eq. (9) represent the contributions of the discrete and continuum excitons, respectively [52,53]. It has been theoretically predicted [48] that in degenerate ZnO, excitonic bound states still exist and affect the absorption line shape even though the values of E_b are negligibly small ($E_b <\approx 0.1$ meV). Indeed, we found that the fitted parameters of E_b are quite small ($E_b \approx 0.5$ meV, see Table I), and the contribution of the first term in Eq. (9) is negligibly small.

We found that the observed room-temperature absorptiokn spectra are well represented by Eq. (8), yielding the fitted values of $E_{\text{th}} = 3.385$ and 3.435 eV for GZO1 and GZO2, respectively (see Table I). However, the absorption spectrum of GZO3 is not fitted to Eq. (8) but can be well represented by the following function taking into account only a Fermi-level filling factor (FLFF) [53,54]:

$$A(E) = A_0(E) \frac{1}{\left\{1 + \exp\left(\frac{E_{\text{abs}} - E}{\text{“}kT\text{”}}\right)\right\} E^2}, \tag{10}$$

where E_{abs} is the absorption edge shifted by the Burstein-Moss effect, the term $\{1 + \exp(\frac{E_{\text{abs}} - E_0}{\text{“}kT\text{”}})\}^{-1}$ is the FLFF, and “kT” is a fitting parameter representing inhomogeneous (temperature) broadening. Hence, it is probable that the expected absorption anomaly is strongly smeared out in GZO3 due to the impurity effect.

If the room-temperature absorption spectra of GZO1 and GZO2 exhibit the FES, it could be possible to observe a similar singularity in the PL and PLE spectra. Unfortunately, the PL emission intensities of GZO1 and GZO2 are too low to recognize the singularity at room temperature when measured by using a spectrofluorometer under Xe lamp excitation. Hence, we performed low-temperature emission and absorption measurements on GZO1 and GZO2 using a He-flow cryostat [Figs. 3(b) and 4]. As for GZO3, however, we did not obtain analyzable PL signals even at temperatures below $\approx$10 K.

First, we investigate the temperature dependence of the optical absorption spectra. We found that the 6-K absorption spectra of GZO1 and GZO2 are well fitted to Eq. (1), as shown in Fig. 3(b), and the fitted values of E_{th} become higher than those at room temperature by $\approx$0.05 eV. Figure 4 also illustrates that a rise feature above the absorption edge is more pronounced for lower temperatures. This is consistent with our interpretation that this rise feature is indicative of the FES.

Next, we analyze the low-temperature PL and PLE characteristics. One sees from Fig. 3(b) that the 6-K PL spectra of GZO1 and GZO2 show an asymmetric emission band peaking at 3.38 eV, whereas the corresponding PLE spectra exhibit a

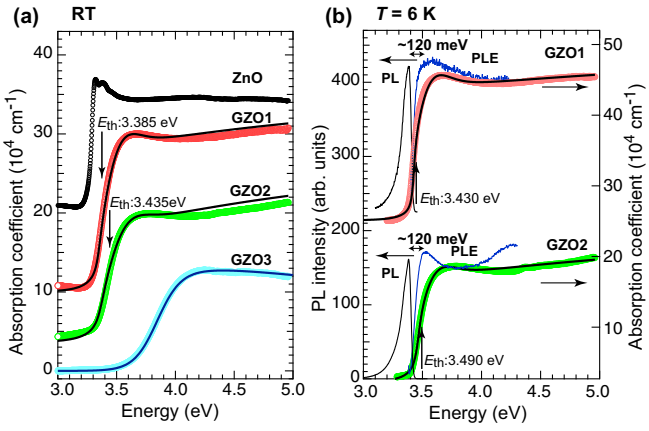

FIG. 3. (a) Room-temperature absorption spectra of ZnO film and three degenerate GZO films, termed GZO1, GZO2, and GZO3. (b) Low-temperature (6 K) absorption, PL and PLE spectra of GZO1 and GZO2. Respective spectra are shifted vertically for clarity. The solid lines for GZO1 and GZO2 are the fit to Eq. (8), showing the fitted values of E_{th}. The solid line for GZO3 is the fit to Eq. (9).

TABLE I. List of fitted parameters in Eqs. (8) and (9) obtained for GZO1 and GZO2 and those in Eqs. (9) and (10) obtained for GZO3.

	Eq. (8)[a]			Eq. (9)		
	α	E_{th} (eV)	Γ_{Gauss} (eV)	E_0	E_b (meV)[b]	Γ_0 (eV)
GZO1 (RT)	0.35	3.385	0.21	3.36	0.5	0.030
GZO1 (6 K)	0.35	3.430	0.20	3.42	0.5	0.016
GZO2 (RT)	0.29	3.435	0.24	3.37	0.5	0.045
GZO2 (6 K)	0.29	3.490	0.20	3.47	0.5	0.031
	Eq. (10)			Eq. (9)		
	E_{abs} (eV)	"kT" (eV)		E_0	E_b (meV)[b]	Γ_0 (eV)
GZO3 (RT)	3.84	0.1		3.37	0.5	0.5

[a]Since the parameter ζ_0 in Eq. (8) hardly modifies the line shape, we do not show the fitted value of ζ_0.
[b]We found that the fitted value of E_b could be less than ≈1 meV. We then fixed the value of E_b as 0.5 meV during the fitting procedures.

rapid increase in intensity at energies above E_{th}, resulting in a peak feature at ≈3.5 eV. We consider that the observation of the ≈3.5-eV peak in the PLE spectra provides additional evidence of the FES in these GZO samples. The PL band at 3.38 eV probably results from the emission from the Fermi edge to the acceptor levels due to Zn vacancy V_{Zn}, which is the main deep acceptor center in n-type ZnO [55]. This is because the observed Stokes shift ΔE of the PL emission

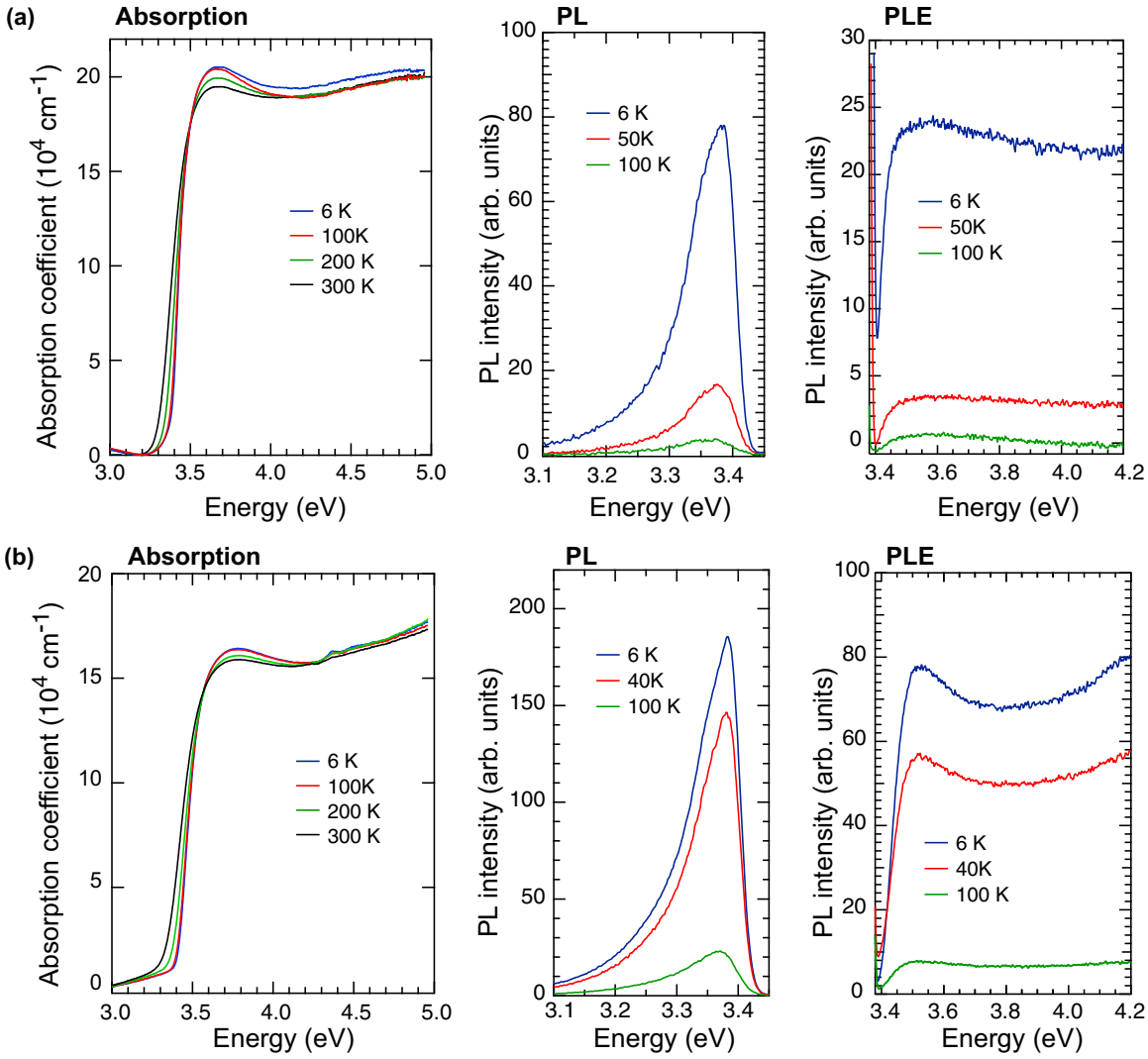

FIG. 4. Temperature dependence of the optical absorption, PL and PLE spectra of (a) GZO1 and (b) GZO2. The measurements were carried out using a Xe lamp as a light source.

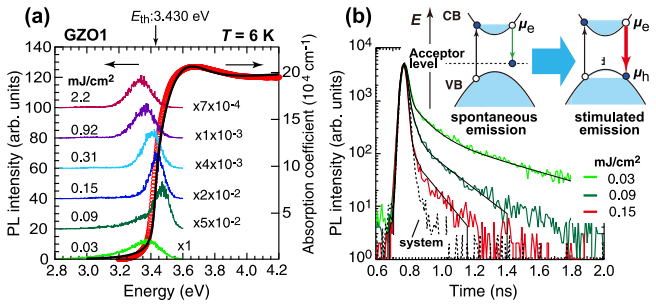

FIG. 5. (a) Left scale: Excitation fluence F_{ex} dependence of the low-temperature (6 K) PL spectra of GZO1 under 100-fs pulse excitation at 332 nm. PL spectra are shifted and scaled by the factor given in the right side of the respective spectra. Right scale: The low-temperature (6 K) absorption coefficient spectrum of GZO1 (red open circles) and the fit to Eq. (8) (solid line), showing the fitted value of E_{th} on the upper horizontal axis. (b) The decay profile of the emission obtained under different excitation fluences indicated. Each solid line represents the fitted convolution curve between the laser pulse and a double exponential function. The fitted decay times (τ_1 and τ_2) under excitation fluences of 0.03, 0.09, and 0.15mJ/cm^2 are 0.10 and 0.50 ns, 0.04 and 0.20 ns, and 0.01 and 0.13 ns, respectively. The inset in (b) schematically shows a transition of the emission process from a spontaneous to a stimulated regime.

with respect to the PLE peak energy ($\Delta E \approx 0.12$ eV) is in good agreement with the ionization energy of the acceptor [$E_A(V_{Zn}) = 0.12$ eV] obtained from density functional calculations [55].

C. Emission characteristics under femtosecond-pulse excitation

In this subsection, we investigate the changes in the PL spectra of the GZO samples with excitation fluence (F_{ex}) under 100-fs pulse excitation at ≈330 nm (≈3.76 eV). The measurements were carried out at 6 K and room temperature. A series of 6-K PL spectra of GZO1 as well as the corresponding absorption spectrum are given in Fig. 5(a). For F_{ex} at 0.03 mJ/cm^2, the PL spectrum shows an asymmetric PL band peaking at ≈3.38eV, in agreement with that obtained using a Xe lamp as an excitation source. When F_{ex} increases from 0.03 to 0.09 mJ/cm^2, the PL spectrum becomes narrow and symmetric, accompanied by a blueshift of the peak energy by ≈0.1 eV along with a significant (more than 20 times) increase in intensity. For higher excitation fluences, a substantial redshift of the peak energy and spectral broadening were observed, as often seen in the stimulated emission from an inverted EHP [5,43]. We also found that the PL decay curves become steeper for F_{ex} larger than 0.09 mJ/cm^2, as shown in Fig. 5(b). These changes in the spectral and decay features with F_{ex} allow us to confirm that a transition from the spontaneous emission to the EHP stimulated emission occurs at the threshold fluence of 0.09 mJ/cm^2, as schematically shown in the inset of Fig. 5(b). Considering that the emission peak energy at the threshold almost coincides with E_{th} (or the PLE peak energy), we can reasonably expect that the resulting stimulated emission is due to the recombination between the electrons at the Fermi edge and the holes in the valence band.

Further noteworthy is that a similar transition from a spontaneous to a stimulated emission regime is seen at room

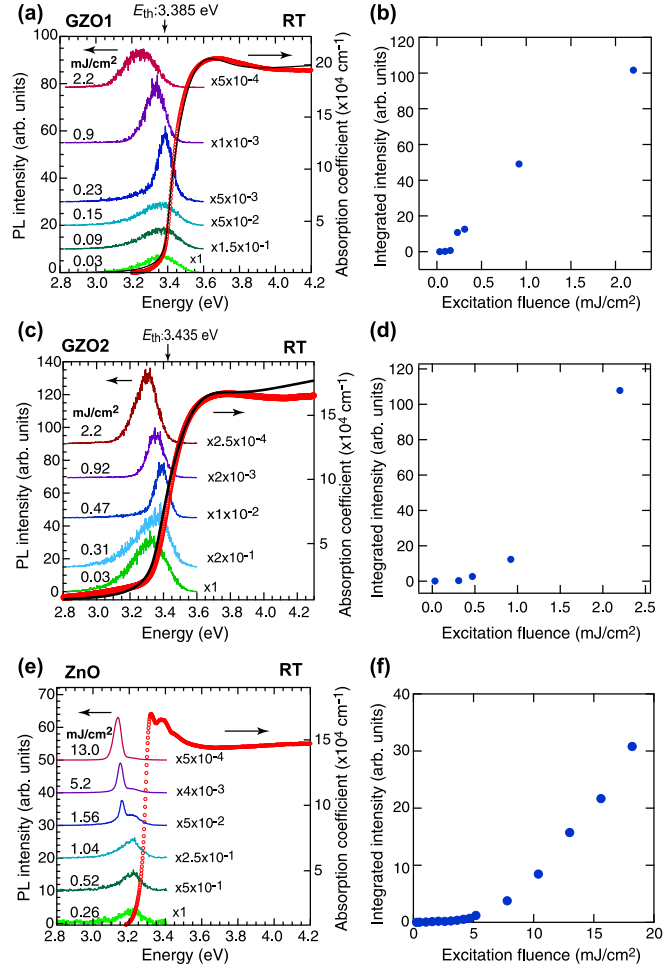

FIG. 6. [(a), (c), (e)] Excitation fluence F_{ex} dependence of the room-temperature PL spectra of (a) GZO1 and (c) GZO2 under 100-fs pulse excitation at 332 nm and (e) ZnO under 10-ns pulse excitation at 355 nm. PL spectra are shifted and scaled by the factor given in the right-hand side of the respective spectra. The corresponding room-temperature absorption coefficient spectra (red open circles) are given in the right scale. The black solid line in (a) and (c) is the fit to Eq. (8), showing the fitted value of E_{th} on the upper horizontal axis. [(b), (d), (f)] The energy-integrated PL intensity of (b) GZO1, (d) GZO2, and (f) ZnO as a function of F_{ex}.

temperature [see Fig. 6(a) for GZO1 and Fig. 6(c) for GZO2]. Here, we should recall that nominally pure ZnO thin films, nanowires, and nanopowders exhibit a room-temperature EHP stimulated emission as well [39–43]. In the case of the ZnO nanostructures, however, the stimulated emission occurs at a lower energy than the spontaneous emission [see, for example, Fig. 6(e)], which is different to the case of GZO1 and GZO2. Note also that the emission peak energy and the half width of GZO1 and GZO2 are substantially higher and broader than those of ZnO although the threshold fluence of GZO1 (≈0.2 mJ/cm^2) and GZO2 (≈0.5 mJ/cm^2) is an order lower than that of ZnO (≈0.2 mJ/cm^2). We assume that these differences in the stimulated emission characteristics between GZO and ZnO originate from the inherently large chemical potential of degenerate semiconductors, as inferred in the Introduction section.

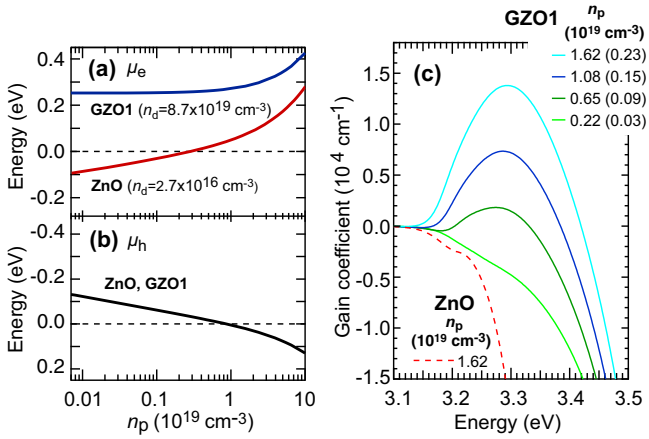

FIG. 7. Changes in (a) μ_e and (b) μ_h as a function of photogenerated electron hole density n_p calculated at 300 K for ZnO and GZO1. The dashed lines in (a) and (b) indicate the reference energy level of the conduction band (conduction band minimum) and that of the valence band (valence band maximum), respectively. (c) Theoretical gain spectra of GZO1 calculated at 300 K for different values of n_p. The values in parentheses represent the corresponding excitation fluences (units in mJ/cm^2) under the present 100-fs excitation condition. The 300-K gain spectrum of ZnO for $n_p = 1.62 \times 10^{19}$cm^{-3} is also shown for comparison.

D. Many-body theory calculations

To confirm the above assumption, we calculated the room-temperature optical gain spectra $g(E)$ of GZO1, i.e., an n-doped ZnO with $n_d = 8.7 \times 10^{19}$cm^{-3}, on the basis of the quantum many-body theory developed by Versteegh *et al.* [46]. The theory was originally developed for the understanding of the optical spectra, charge-carrier screening, and carrier dynamics of ZnO at room temperature in the course of optical excitation, in which the net densities of electron n and hole p under photoexcitation are both equal to n_p. The theory is applicable to the photoexcited system with $n < 2.8 \times 10^{20}$cm^{-3} [46], where charge-carrier screening is established fast with respect to the Fermi frequencies. Hence, we believe that this many-body theory is useful to understand the gain characteristics of degenerate systems at room temperature. In addition, μ_e and μ_h, both of which are required to calculate the screening length and the susceptibility in the framework of the quantum many-body theory [44–46], were numerically determined within the parabolic band approximation, as described in Sec. II C.

Figure 7(a) shows how μ_e and μ_h of GZO1 ($n_d = 8.7 \times 10^{19}$cm^{-3}) change as n_p increases at a temperature of 300 K. For comparison, we also show in Fig. 7(a) the results on the ZnO sample with n_d of 2.7×10^{16}cm^{-3}. One sees from Fig. 7(a) that in GZO1, μ_e is already situated well above the bottom of the corresponding bands ($\mu_e \approx 0.25$eV) even for $n_p < 1 \times 10^{17}$cm^{-3}, whereas, in ZnO, μ_e does not become positive until n_p reaches $\approx 2 \times 10^{18}$cm^{-3}. On the other hand, the μ_h values in ZnO and GZO1 practically show the same n_p dependence, becoming positive for $n_p > \approx 1 \times 10^{19}$cm^{-3}. These changes in μ_e and μ_h with n_p are reflected in the n_p dependence of $g(E)$, as shown in Fig. 7(b). As for GZO1 film with $D = 236$ nm, the photogenerated electron-hole pair density n_p at the room-temperature threshold fluence ($F_{ex} = 0.23$ mJ/cm^2) is estimated to be $n_p = 1.62 \times 10^{19}$cm^{-3} from $n_p = F_{ex}/(\hbar\omega D)$ [44], where $\hbar\omega$ is the photon energy of the pump laser. It is clear from Fig. 7(b) that in GZO1, an optical gain appears at $n_p = 6.5 \times 10^{18}$ cm^{-3} and reaches $\approx 1.4 \times 10^4$ cm^{-1} at 3.3 eV for $n_p = 1.62 \times 10^{19}$cm^{-3}. The resulting gain spectra are in reasonable agreement with the symmetric PL spectra observed for $F_{ex} \geqslant 0.23$ mJ/cm^2 shown in Fig. 6(a). Although the present calculations yield the theoretical upper bound for $g(E)$, these calculations support the occurrence of room-temperature stimulated emission from the GZO film in the present experimental condition. Note also that in ZnO, no gain occurs for $n_p = 1.62 \times 10^{19}$cm^{-3}. These calculated results are consistent with the difference of EHP stimulated emission characteristics between GZO and ZnO shown in Fig. 6, i.e., a lower threshold, a broader spectral width, and a higher peak energy of GZO than those of ZnO.

IV. CONCLUSIONS

High-quality degenerate GZO films with n_d of $\approx 1 \times 10^{20}$cm^{-3} show a signature of the FES in the absorption and PLE spectra, along with the EHP stimulated emission not only at cryogenic, but also at room temperature under the above-band-gap pulsed laser excitation conditions. At the threshold, the stimulated emission occurs at higher energies with respect to the spontaneous emission, yielding the peak energy corresponding to the Fermi-edge energy inferred from the absorption and PLE spectra. We then performed quantum many-body calculations to estimate the theoretical upper bound of the optical gain in GZO1 at room temperature. For the same value of n_p, GZO1 yields a much higher EHP gain than ZnO. Also, the calculated gain spectra of GZO1 are basically in agreement with the observed stimulated emission spectra. Hence, the present results demonstrate the transition of the Fermi-edge emission from a spontaneous to a stimulated regime, shedding light on the absorption and emission processes in dense electron-hole systems in view of FES.

[1] G. D. Mahan, *Many-Particle Physics*, 3rd ed. (Plenum, New York, 2000).
[2] P. Coleman, *Introduction to Many-Body Physics* (Cambridge University, Cambridge, England, 2016).
[3] D. S. Chemla and J. Shah, Many-body and correlation effects in semiconductors, Nature (London) **411**, 549 (2001).
[4] M. Kira and S. W. Koch, Many-body correlations and excitonic effects in semiconductor spectroscopy, Prog. Quantum Electron. **30**, 155 (2006).
[5] C. F. Klingshirn, *Semiconductor Optics*, 2nd ed. (Springer-Verlag, Berlin, 2005), pp. 521–552.
[6] G. D. Mahan, Excitons in degenerate semiconductors, Phys. Rev. **153**, 882 (1967).

[7] G. D. Mahan, Excitons in metals: Infinite hole mass, Phys. Rev. **163**, 612 (1967).

[8] M. Feneberg, S. Osterburg, K. Lange, C. Lidig, B. Garke, R. Goldhahn, E. Richter, C. Netzel, M. D. Neumann, N. Esser, S. Fritze, H. Witte, J. Bläsing, A. Dadgar, and A. Krost, Band gap renormalization and Burstein-Moss effect in silicon- and germanium-doped wurtzite GaN up to 10^{20} cm^{-3}, Phys. Rev. B **90**, 075203 (2014).

[9] F. Fuchs, K. Kheng, P. Koidl, and K. Schwarz, Fermi-edge singularity in degenerate n-type bulk InAs, Phys. Rev. B **48**, 7884 (1993).

[10] T. Makino, K. Tamura, C. H. Chia, Y. Segawa, M. Kawasaki, A. Ohtomo, and H. Koinuma, Optical properties of ZnO:Al epilayers: Observation of room-temperature many-body absorption-edge singularity, Phys. Rev. B **65**, 121201(R) (2002).

[11] P. Karnatak, S. Goswami, V. Kochat, A. N. Pal, and A. Ghosh, Fermi-edge transmission resonance in graphene driven by a single coulomb impurity, Phys. Rev. Lett. **113**, 026601 (2014).

[12] N. A. J. M. Kleemans, J. van Bree, A. O. Govorov, J. G. Keizer, G. J. Hamhuis, R. Nötzel, A. Yu. Silov, and P. M. Koenraad, Many-body exciton states in self-assembled quantum dots coupled to a Fermi sea, Nat. Phys. **6**, 534 (2010).

[13] P. Plochocka-Polack, J. G. Groshaus, M. Rappaport, V. Umansky, Y. Gallais, A. Pinczuk, and I. Bar-Joseph, Fermi-edge singularity of spin-polarized electrons, Phys. Rev. Lett. **98**, 186810 (2007).

[14] J.-H. Kim, G. T. Noe II, S. A. McGill, Y. Wang, A. K. Wójcik, A. A. Belyanin, and J. Kono, Fermi-edge superfluorescence from a quantum-degenerate electron-hole gas, Sci. Rep. **3**, 3283 (2013).

[15] T. Palmieri, E. Baldini, A. Steinhoff, A. Akrap, M. Kollár, E. Horváth, L. Forró, F. Jahnke, and M. Chergui, Mahan excitons in room-temperature methylammonium lead bromide perovskites, Nat. Commun. **11**, 850 (2020).

[16] S. Gao, Y. Liang, C. D. Spataru, and L. Yang, Dynamical excitonic effects in doped two-dimensional semiconductors, Nano Lett. **16**, 5568 (2016).

[17] D. Pimenov and M. Goldstein, Spectra of heavy polarons and molecules coupled to a Fermi sea, Phys. Rev. B **98**, 220302(R) (2018).

[18] D. J. Choksy, E. A. Szwed, L. V. Butov, K. W. Baldwin, and L. N. Pfeiffer, Fermi edge singularity in neutral electron–hole system, Nat. Phys. **19**, 1275 (2023).

[19] Y.-W. Chang and D. R. Reichman, Many-body theory of optical absorption in doped two-dimensional semiconductors, Phys. Rev. B **99**, 125421 (2019).

[20] C. Jackson and B. Braunecker, Spatiotemporal spread of Fermi-edge singularity as time-delayed interaction and impact on time-dependent RKKY-type coupling, Phys. Rev. Res. **4**, 013119 (2022).

[21] H. van Cong, S. Charar, and S. Brunet, Band-gap narrowing due to many body effects in *n*-Type degenerate GaAs crystals, Phys. Status Solidi B **147**, 253 (1988).

[22] D. M. Szmyd, P. Porro, A. Majerfeld, and S. Lagomarsino, Heavily doped GaAs:Se. I. Photoluminescence determination of the electron effective mass, J. Appl. Phys. **68**, 2367 (1990).

[23] H. D. Chen, M. S. Feng, P. A. Chen, K. C. Lin, and C. C. Wu, Low-temperature luminescent properties of degenerate p-type GaAs grown by low-pressure metalorganic chemical vapor deposition, J. Appl. Phys. **75**, 2210 (1994).

[24] M. A. Reshchikov and H. Morkoç, Luminescence properties of defects in GaN, J. Appl. Phys. **97**, 061301 (2005).

[25] K. Ueno, T. Fudetani, Y. Arakawa, A. Kobayashi, J. Ohta, and H. Fujioka, Electron transport properties of degenerate n-type GaN prepared by pulsed sputtering, APL Mater. **5**, 126102 (2017).

[26] S. Shokhovets, K. Köhler, O. Ambacher, and G. Gobsch, Observation of Fermi-edge excitons and exciton-phonon complexes in the optical response of heavily doped *n*-type wurtzite GaN, Phys. Rev. B **79**, 045201 (2009).

[27] H. P. He, H. P. Tang, Z. Z. Ye, L. P. Zhu, B. H. Zhao, L. Wang, and X. H. Li, Temperature-dependent photoluminescence of quasi aligned Al-doped ZnO nanorods, Appl. Phys. Lett. **90**, 023104 (2007).

[28] Z. Yang, D. C. Look, and J. L. Liu, Ga-related photoluminescence lines in Ga-doped ZnO grown by plasma-assisted molecular-beam epitaxy, Appl. Phys. Lett. **94**, 072101 (2009).

[29] H. C. Park, D. Byun, B. Angadi, D. Hee Park, W. K. Choi, J. W. Choi, and Y. S. Jung, Photoluminescence of Ga-doped ZnO film grown on c-Al_2O_3 (0001) by plasma-assisted molecular beam epitaxy, J. Appl. Phys. **102**, 073114 (2007).

[30] T. Makino, Y. Segawa, S. Yoshida, A. Tsukazaki, A. Ohtomo, and M. Kawasaki, Gallium concentration dependence of room-temperature near-band-edge luminescence in *n*-type ZnO:Ga, Appl. Phys. Lett. **85**, 759 (2004).

[31] M. S. Skolnick, J. M. Rorison, K. J. Nash, D. J. Mowbray, P. R. Tapster, S. J. Bass, and A. D. Pitt, Observation of a many-body edge singularity in quantum-well luminescence spectra, Phys. Rev. Lett. **58**, 2130 (1987).

[32] H. Kalt, K. Leo, R. Cingolani, and K. Ploog, Fermi-edge singularity in heavily doped GaAs multiple quantum wells, Phys. Rev. B **40**, 12017(R) (1989).

[33] W. Chen, M. Fritze, W. Walecki, A. V. Nurmikko, D. Ackley, J. M. Hong, and L. L. Chang, Excitonic enhancement of the Fermi-edge singularity in a dense two-dimensional electron gas, Phys. Rev. B **45**, 8464 (1992).

[34] V. Huard, R. T. Cox, K. Saminadayar, A. Arnoult, and S. Tatarenko, Bound states in optical absorption of semiconductor quantum wells containing a two-dimensional electron gas, Phys. Rev. Lett. **84**, 187 (2000).

[35] H. Kissel, U. Zeimer, A. Maaßdorf, M. Weyers, R. Heitz, D. Bimberg, Yu. I. Mazur, G. G. Tarasov, Vas. P. Kunets, U. Müller, Z. Ya. Zhuchenko, and W. T. Masselink, Behavior of the Fermi-edge singularity in the photoluminescence spectra of a high-density two-dimensional electron gas, Phys. Rev. B **65**, 235320 (2002).

[36] M. G. A. Bernard and G. Duraffourg, Laser conditions in semiconductors, Phys. Status Solidi B **1**, 699 (1961).

[37] J. I. Pankove, *Optical Processes in Semiconductors* (Dover, New York, 1971), p. 216.

[38] L. Carroll, P. Friedli, S. Neuenschwander, H. Sigg, S. Cecchi, F. Isa, D. Chrastina, G. Isella, Y. Fedoryshyn, and J. Faist, Direct-gap gain and optical absorption in germanium correlated to the density of photoexcited carriers, doping, and strain, Phys. Rev. Lett. **109**, 057402 (2012).

[39] C. Klingshirn, ZnO: From basics towards application, Phys. Stat. Sol. B **244**, 3027 (2007).

[40] *Zinc Oxide: From Fundamental Properties Towards Novel Applications*, edited by C. F. Klingshirn, B. K. Meyer, A. Waag, A.

Hoffmann, and J. Geurts, Springer Series in Materials Science (Springer-Verlag, Berlin, 2010).

[41] *Zinc Oxide: Fundamentals, Materials and Device Technology*, edited by H. Morkoç and Ü. Özgür (Wiley, New York, 2009).

[42] *Zinc Oxide Materials for Electronic and Optoelectronic Device Applications*, edited by C. Litton, D. C. Reynolds, and T. C. Collins (Wiley, New York, 2011).

[43] A. Tashiro, Y. Adachi, and T. Uchino, Excitonic processes and lasing in ZnO thin films and micro/nanostructures, J. Appl. Phys. **133**, 221101 (2023).

[44] M. A. M. Versteegh, D. Vanmaekelbergh, and J. I. Dijkhuis, Room-temperature laser emission of ZnO nanowires explained by many-body theory, Phys. Rev. Lett. **108**, 157402 (2012).

[45] T. Nakamura, K. Firdaus, and S. Adachi, Electron-hole plasma lasing in a ZnO random laser, Phys. Rev. B **86**, 205103 (2012).

[46] M. A. M. Versteegh, T. Kuis, H. T. C. Stoof, and J. I. Dijkhuis, Ultrafast screening and carrier dynamics in ZnO: Theory and experiment, Phys. Rev. B **84**, 035207 (2011).

[47] E. Hendry, M. Koeberg, and M. Bonn, Exciton and electron-hole plasma formation dynamics in ZnO, Phys. Rev. B **76**, 045214 (2007).

[48] A. Schleife, C. Rödl, F. Fuchs, K. Hannewald, and F. Bechstedt, Optical absorption in degenerately doped semiconductors: Mott transition or Mahan excitons? Phys. Rev. Lett. **107**, 236405 (2011).

[49] For example see, N. A. Shepelin, Z. P. Tehrani, N. Ohannessian, C. W. Schneider, D. Pergolesi, and T. Lippert, A practical guide to pulsed laser deposition, Chem. Soc. Rev. **52**, 2294 (2023).

[50] P. Fons, K. Iwata, A. Yamada, K. Matsubara, S. Niki, K. Nakahara, T. Tanabe, and H. Takasu, Uniaxial locked epitaxy of ZnO on the a face of sapphire, Appl. Phys. Lett. **77**, 1801 (2000).

[51] Y. Xie, M. Madel, T. Zoberbier, A. Reiser, W. Jie, B. Neuschl, J. Biskupek, U. Kaiser, M. Feneberg, and K. Thonke, Enforced c-axis growth of ZnO epitaxial chemical vapor deposition films on *a*-plane sapphire, Appl. Phys. Lett. **100**, 182101 (2012).

[52] A. R. Goni, A. Cantarero, K. Syassen, and M. Cardona, Effect of pressure on the low-temperature exciton absorption in GaAs, Phys. Rev. B **41**, 10111 (1990).

[53] M. Muñoz, F. H. Pollak, M. Kahn, D. Ritter, L. Kronik, and G. M. Cohen, Burstein-Moss shift of n-doped $In_{0.53}Ga_{0.47}As/InP$, Phys. Rev. B **63**, 233302 (2001).

[54] J. D. Ye, S. L. Gu, S. M. Zhu, S. M. Liu, Y. D. Zheng, R. Zhang, and Y. Shi, Fermi-level band filling and band-gap renormalization in Ga-doped ZnO, Appl. Phys. Lett. **86**, 192111 (2005).

[55] A. Janotti and C. G. Van de Walle, Native point defects in ZnO, Phys. Rev. B **76**, 165202 (2007).